Competition between shear localization and tensile detwinning in twinned nanowires

Sheng Yin,[1,3,*] Guangming Cheng,[2,4,*] Yong Zhu,[2,†] and Huajian Gao[1,5,‡]
[1]*School of Engineering, Brown University, Providence, Rhode Island 02912, USA*
[2]*Department of Mechanical and Aerospace Engineering, North Carolina State University, Raleigh, North Carolina 27695, USA*
[3]*Department of Materials Science and Engineering, University of California, Berkeley, California 94720, USA*
[4]*Princeton Institute for the Materials Science and Technology, Princeton University, Princeton, New Jersey 08540, USA*
[5]*School of Mechanical and Aerospace Engineering, College of Engineering, Nanyang Technological University, 70 Nanyang Drive, Singapore 637457, Singapore*

(Received 2 January 2020; accepted 10 February 2020; published 24 February 2020)

Recently, a transition of deformation mechanism from localized dislocation slip to delocalized plasticity via an anomalous tensile detwinning mechanism has been discovered in bitwinned metallic nanowires (NWs) with a single twin boundary (TB) running parallel to the NW length. However, experiments showed that the anomalous tensile detwinning in most of bitwinned NWs does not propagate through the whole NW, which limits the NWs failure strain when compared to the twinning-induced superplasticity in single-crystalline NWs. An elusive but fundamentally important question is that what factors might affect the propagation of tensile detwinning in such bitwinned NWs. In addition, can this tensile detwinning mechanism be applied to other types of twinned NWs? Here, based on *in situ* transmission electron microscopy testing and molecular dynamics simulations, a competition between shear localization and tensile detwinning is identified. By dividing the tensile detwinning mechanism into two steps and investigating each step separately, it is found that the quality of a single-crystalline embryo formed during step one determines the succeeding detwinning propagation (step two) and the final plastic strain. Furthermore, this anomalous tensile detwinning mechanism is extended to other metallic NWs with multiple TBs running parallel to the length direction, such as asymmetric pentatwinned NWs and NWs with multiple parallel TBs. This work highlights the important role of detwinning in large plasticity in metallic NWs with different twin structures.

DOI: 10.1103/PhysRevMaterials.4.023603

I. INTRODUCTION

Metallic nanowires (NWs) are among the most important building blocks for a variety of applications such as flexible/stretchable electronics, transparent electrodes, sensors, optoelectronics, and nanoelectromechanical systems [1–5]. Mechanical properties of metallic NWs are of critical importance to the operation and reliability of the NW-based devices. In contrast to the forest dislocation dynamics in bulk materials, surface dislocation nucleation has been identified as a dominant deformation mechanism in metallic NWs [6–21]. NWs with internal microstructure such as twin boundaries (TBs) have received much interest recently due to their high strength (higher than single-crystalline counterparts) [22,23], strain hardening [24], and recoverable plasticity and Bauschinger effect [25]. However, twinned NWs often showed limit fracture strain of less than a few percent owing to shear localization [17,23]. How to improve the ductility of such NWs is a question that has recently attracted attention owing to its importance for the design of functional and reliable NW-based devices [25,26].

TBs have been shown to be able to simultaneously enhance the strength, ductility and fracture toughness of bulk metals [27,28], ceramics [29–31], biomaterials [32], and more recently twinned metallic NWs [23–25,33–35]. Detwinning, as an important deformation mode in nanotwinned metals, has been observed both experimentally and in computational simulations [22,36–40]. For example, detwinning has been observed in Cu nanopillars [22] and Au NWs [37] with preexisting TBs inclined with respect to the loading directions. Proposed mechanisms including cross-slip of partial dislocations at the TB [38] and migration of incoherent TBs formed by twinning partials [36,40]. The key to detwinning is nucleation of twinning partials on a TB. In all these cases, a finite resolved shear stress is needed for the detwinning process. In contrast, a tensile detwinning mechanism was recently reported in bitwinned metallic NWs, which is unique in that the loading direction is parallel to the twin plane and there is no resolved shear stress along the TB at the initial stage [23]. This novel tensile detwinning mechanism was identified to start with multiple dislocation interactions with the TB and nucleation of a single-crystalline embryo, followed by propagation of the single-crystalline embryo, leading to large plastic deformation. However, the tensile detwinning in most of the bitwinned NWs did not propagate as far as in the case of the twinning-induced superplasticity in single-crystalline NWs. Two important questions arise: (1) what factors might affect the propagation of tensile detwinning in such NWs

*These authors contributed equally to this work.
†yong_zhu@ncsu.edu
‡huajian.gao@ntu.edu.sg

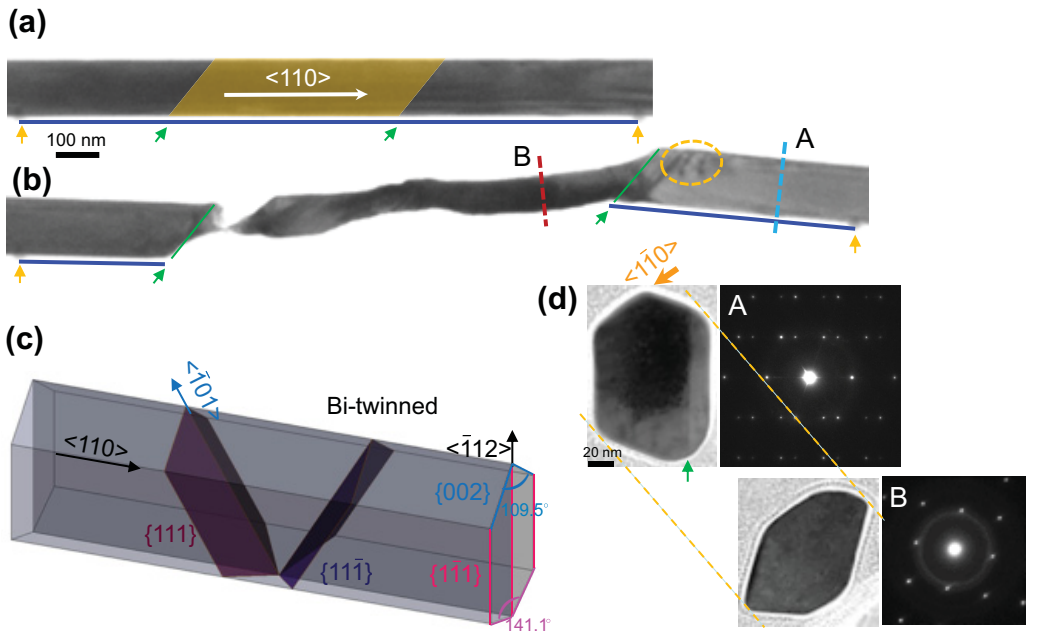

FIG. 1. Microstructure characterization of a bitwinned NW before and after plastic deformation [23]. [(a) and (b)] Large plasticity observed in a bitwinned NW with small volume ratio undergoing tensile detwinning deformation: (a) before tensile testing and (b) after tensile detwinning deformation. Two displacement markers for strain measurement are labeled by orange arrows. The yellow marked area in (a) correspond to the deformed parts in (b) labeled by green arrows. Localized dislocations are marked by dashed oval in (b). TEM observation is along $\langle 1\bar{1}0\rangle$ of the dominant twin variant as marked in (d) dashed lines in (b) marked the positions for the cross-sectional TEM images in (d). (c) Schematic drawings of bitwinned structure with length along $\langle 110\rangle$ direction. (d), Corresponding cross-sectional TEM images and diffraction patterns of the tested NW before and after plastic deformation in (a) and (b). The TB was marked by green arrow.

that limit their plasticity? And (2) how does this delocalizing tensile detwinning mechanism generally operate in NWs with multiple parallel TBs?

Here, based on *in situ* transmission electron microscopy (TEM) testing and molecular dynamics (MD) simulations, we identify the existence of a competition between shear localization and tensile detwinning in bitwinned NWs. By dividing the tensile detwinning mechanism into two steps and investigating each step separately, we find the quality of a single-crystalline embryo formed during the first step determines the succeeding detwinning propagation (step two) and the final plastic strain. In addition, we find that the novel two-step tensile detwinning mechanism is operative in several other metallic NWs with multiple TBs running parallel to the length direction, such as the NWs with multiple parallel TBs and the asymmetric pentatwinned NWs as observed in experiments.

II. METHODOLOGY

A. Experimental procedures

Sample synthesis and characterization. Crystalline Ag NWs were synthesized by physical vapour deposition inside a molecular beam epitaxy system under ultrahigh vacuum condition and substrate temperature of 700 °C. More details of the NW synthesis process are provided elsewhere [41].

Cross-sectional TEM samples of Ag NWs before and after deformation were prepared with focused ion beam (FIB). High-resolution TEM observations were performed on JEOL 2010F with a Schottky field emission gun (FEG) operated at 200 kV. Atomic resolution high-angle annular dark-field (HAADF) scanning transmission electron microscopy (STEM) imaging was performed on a probe corrected FEI Titan G^2 60–300 kV S/TEM equipped with an X-FEG source operated at 200 kV.

In situ SEM/TEM mechanical testing. The mechanical testing of NWs as shown by Figs. 1(a) and 1(b) was carried out *in situ* inside a TEM using a MEMS-based material testing stage, which consists of an electrostatic (comb-drive) actuator and a capacitive load sensor, with a gap in between for mounting samples. Details of the testing stage have been reported previously [42–44]. Displacement (and strain) is measured by digital image correlation of TEM images of two local markers on the specimen. This MEMS-based testing stage has a strain resolution of 0.01% (gage length 2 μm) and a stress resolution of 1.4 MPa (for example, for NW diameter of 104 nm [25]).

NWs were mounted on the testing stage using a nanomanipulator (Klocke Nanotechnik, Germany) inside a FEI Nova 600 dual beam. A single Ag NW was welded to the nanomanipulator probe, then mounted to the MEMS stage and clamped by electron-beam-induced Pt deposition at the two free ends. Two local markers were deposited on the NWs for displacement (and strain) measurement. *In situ* TEM mechanical testing was performed on JEOL 2010F operated at 200 kV. The loading and unloading strain rates were ~0.003%/s. Low magnification images were recorded at a fixed condense (the second condense lens) current to minimize the focus change. The current density of incident e-beam is <0.1 A/cm^2 and its effect on the mechanical behavior of the NW under tensile testing can be neglected.

B. Modelling

Large-scale MD simulations were performed using the software package LAMMPS [45]. The embedded atom method (EAM) potential for Ag [46] was used to describe the interatomic interactions in all the simulations. In addition, to show that the key mechanism and results are independent of the used potential, simulations shown in Fig. 6 and part of the pentatwinned NWs simulations were repeated in other two different EAM potentials, including a classic EAM potential developed by Adams *et al.* [47] and a recently developed EAM potential by Pan *et al.* [48] that can correctly reproduce the stable and unstable stacking fault energies in Ag. All these potentials can get consistent results as shown in Fig. 6 and transition from slip to tensile detwinning in pentatwinned NW. Periodic boundary condition was imposed along the axial direction (that is, the loading direction ⟨110⟩) of all simulated samples. The length of all the simulated NWs were 80 nm. For cross-sections of NWs, the W is around 13 nm and H ranges from 5 to 12 nm. The total number of atoms in each simulation ranges from 0.3 to 0.7 million. The samples were initially relaxed and equilibrated at temperature of 300 K for 800 ps using the Nosé-Hoover [49] thermostat and barostat, followed by stretch at a constant strain rate of $10^8\,s^{-1}$ under NVT ensemble (canonical ensemble) until failure. To visualize defects generated during deformation, atoms were painted with different crystalline order in different colors using a common neighbor analysis by OVITO [50]. The green-colored atoms stand for atoms with face-centered cubic symmetry, the red ones those with hexagonal close-packed symmetry and the grey ones those at dislocation cores, free surfaces and surfaces defects.

III. RESULTS AND DISCUSSIONS

A. Tensile detwinning in bitwinned Ag NWs

Bitwinned NWs with a single TB running parallel to the NW length direction (Fig. 1) was found to be dominant (81% in the examined 113 NWs) in the crystalline Ag NWs synthesized by physical vapor deposition [23,41]. Figure 1(c) shows schematically a bitwinned NW with the axial direction of ⟨110⟩. Two twin variants are distributed at the two sides of the TB with symmetrical arrangement of crystal planes such as the marked {111} and $\{11\bar{1}\}$ in Fig. 1(c).

It has been reported that the deformation modes in the bitwinned NWs are affected by the cross-sectional aspect ratio and the volume ratio between the two twin variants [23] (r defined as V_{small}/V_{large}). Tensile detwinning deformation was identified to lead to the observed large plasticity in bitwinned NWs with a small volume ratio of 0.19 [Figs. 1(a) and 1(b)], which was different from both the twinning-induced superplasticity in single-crystalline NWs [51] and the localized dislocation slip in bitwinned NWs with large volume ratio [23]. During the tensile detwinning process, a new single-crystalline phase was formed and propagate along the NW length, reorienting the NW to the ⟨001⟩ direction [see the cross-sectional TEM image and corresponding diffraction pattern in Fig. 1(d)]. As shown in Fig. 1(b), there was an elongation of 56.8% measured from the two ends marked by green arrows (single-crystalline phase) in the bitwinned NW [Fig. 1(d)]. The large elongation can be attributed to the cross-sectional change, an area shrinkage of 36% [comparing locations A and B in Fig. 1(b)] during the plastic deformation, as shown in Fig. 1(d). Note that there is no obvious change of the dimension along $\langle 1\bar{1}0\rangle$ orientation but a large size shrinkage along the direction perpendicular to $\langle 1\bar{1}0\rangle$ orientation (38.5%).

B. Competition of shear localization and tensile detwinning

It is worth noting that in most of the experiments, the tensile detwinning process, even in bitwinned NWs with small volume ratio, did not propagate far prior to failure, for instance, when compared to the coherent twinning propagation in single-crystalline NWs. In Fig. 1(b), upon failure of the NW, we can clearly distinguish the detwinned region in the middle (between the two green arrows) and the bitwinned part at the two ends of NW. The detwinning did not propagate through the whole NW before localized failure occurred.

Figure 2 shows the MD simulation results of two typical cases of tensile detwinning in bitwinned NWs with different cross-section geometry (H/W and r). In case i, the whole NW was detwinned, leading to an overall 45% elongation, whereas in case ii, after a certain level of tensile detwinning, shear localization occurred in the detwinned region and led to failure by necking (with an overall fracture strain of 28%). From the experiment and MD simulations, we can observe that in some cases, tensile detwinning can propagate through the whole NW, leading to large plasticity as in the case of single-crystalline NWs. While in most cases, shear localization and failure occur close to the initial detwinning site before the whole NW is detwinned. This can be attributed to the competition between shear localization and tensile detwinning in bitwinned NWs. Our hypothesis is that the defects created along with nucleation of single-crystalline embryo (step-one detwinning) as well as the initial surface roughness of the NW might introduce stress concentrations and localized dislocations slip, which would compete with migration of the single-crystalline phase and prevent further tensile detwinning.

During the step-one detwinning, the reactions between the surface-nucleated dislocations and the TB lead to the creation of a single-crystalline embryo. However, under high tensile stress, dislocations are usually nucleated at multiple sites at the same time and some of them can take place near the detwinning embryo region. As shown by the green dashed circle in Fig. 3(a), close to the detwinned region, there are many surface slip traces left in the NW after the step-one detwinning. Figure 3(b) shows the detailed structure of defects created during the step-one detwinning in the NW by showing only HCP atoms. Under further loading, the step-two detwinning takes over until the TB-GB-TB structure meets the defects indicated by the green dashed circle. Dislocation slip will compete with tensile detwinning at the green dashed circle region, which can lead to shear localization. Tensile detwinning cannot propagate further due to the defects created during the step-one detwinning.

Besides the defects created during step-one detwinning, initial surface roughness in the NW might also serve as an obstacle to tensile detwinning. To explore the surface

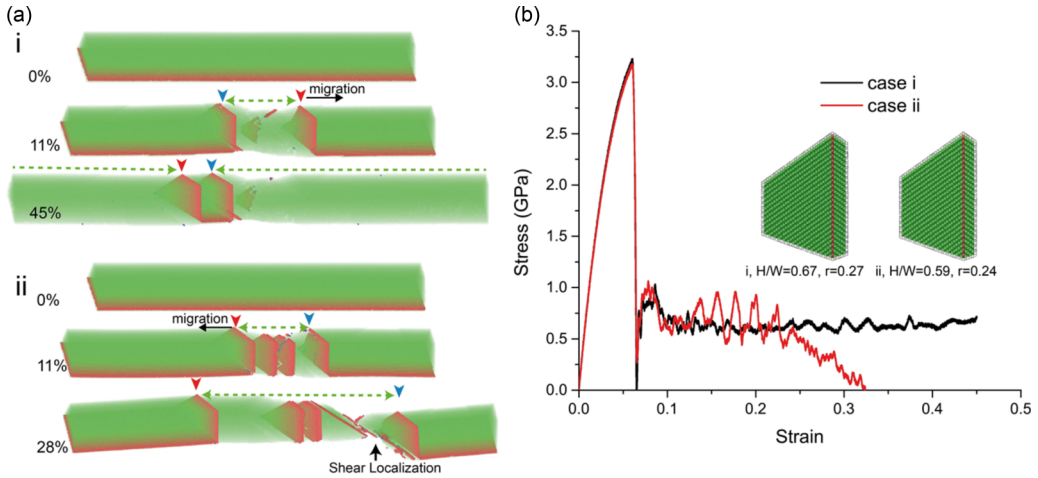

FIG. 2. Different levels of plasticity in bitwinned NWs. (a) Snapshots of detwinning process in two different cases. Green dashed line indicates the detwinned region. The blue and red arrows mark the two ends of the single-crystalline region. Periodic boundary condition was imposed along the axial direction of the NWs. In case i, the TB-GB junction indicated by the red arrow migrated rightward to detwin the NW; it went through the periodic boundary at the end until meeting the blue arrow. Finally, the whole NW is detwinned with an overall elongation of 45%. In case ii, after a certain amount of tensile detwinning, shear localization occurred in the detwinned region leading to failure by necking (with a fracture strain of 28%), as indicated by the black arrow. (b) Stress-strain curves of the two different bitwinned cases in (a).

roughness effect, instead of a pristine bitwinned NW, we introduce several surface notches on the {111} surfaces of the NW. The test case is identical to the NW shown in Fig. 2(a) except for the notches that are 0.5 nm in depth and 0.6 nm in width, as shown by the red arrows in Fig. 4(a). Figure 4(b) shows the structure of the NW at failure. Different from the fully tensile detwinning without surface defects in Fig. 2(a), the NW fails through localized shear at a partial detwinning state. By carefully examining the deformation process, we observe that the initial dislocations favor nucleation at the notches. More necking and dislocation nucleation at multiple notched sites occur before the step-one detwinning. These extra dislocation activities prevent step-one detwinning from completion and as a result shear localization dominates early, leading to partial tensile detwinning in the NW as shown in Fig. 4(b).

The above results have shown the importance of surface roughness and defects created during the step-one detwinning in mediating the competition between shear localization and tensile detwinning. In the following, by decoupling the tensile detwinning process in MD simulations, we will further elucidate and discuss the competition between shear localization and tensile detwinning in some detail.

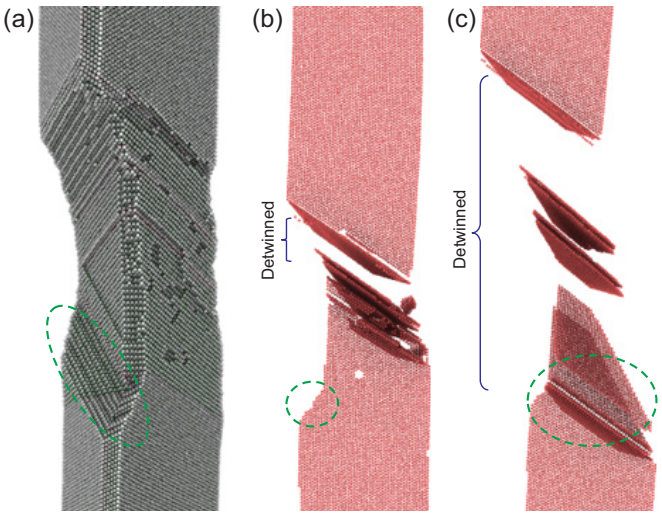

FIG. 3. Defects created during step-one detwinning. (a) The surface of the deformed region of the NW after step-one detwinning. Green dashed circle indicates slip traces created by full dislocations during step-one detwinning. (b) The same structure of (a) but only the HCP atoms are shown. Green dashed circle indicates defects created during step-one detwinning. The detwinning region is also marked by blue bracket. (c) Shear localization occurred as tensile detwinning propagated to the green circle marked region.

C. Decoupling of the two steps in tensile detwinning

MD simulation results have revealed that the tensile detwinning can be described a two-step process [23], as shown in Fig. 5(a). The step-one detwinning involves multiple dislocation reactions to nucleate a single-crystalline embryo,

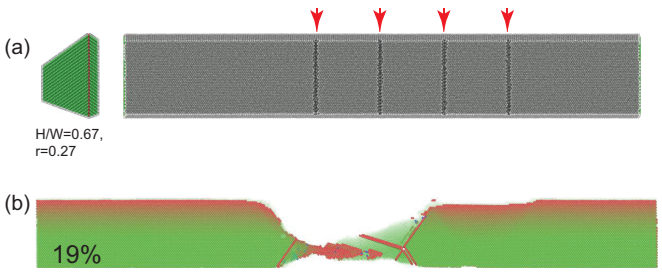

FIG. 4. Deformation of bitwinned NW with external surface roughness. (a) The NW used here is one that can be fully detwinned as shown in Fig. 2(a). Red arrows show surface notches on {111} facets (depth: 0.5 nm, width: 0.6 nm). (b) The NW failed at strain 19% by localized shear. Detwinning cannot propagate due to the presence of the notches.

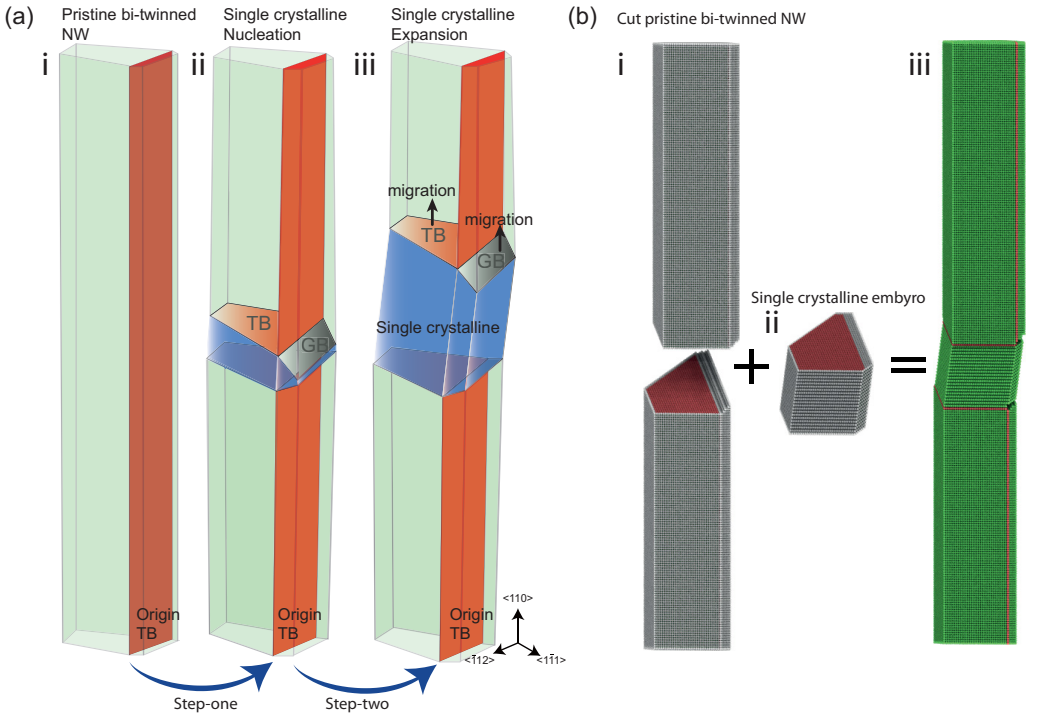

FIG. 5. Direct construction of the NW atomic structure after step-one detwinning by crystalline geometry. (a) Schematic figures showing the step-one detwinning process [23]. (b) Cut the bitwinned NW (b,i) and then weld the remaining NW (b,i) and a single-crystalline embryo (b,ii) according to the unique TB-GB-TB structure observed during the step-one tensile detwinning process. (b,iii) shows the bitwinned NW with the single-crystalline embryo. The periodic boundary condition is kept in the axial direction by slight tilting the NW to match the two ends and followed an energy minimization process. Colored in CNA method where green represents perfect FCC atoms and red represents HCP atoms.

which is considered to be the key to the success of the succeeding deformation. If the bitwinned NW cannot overcome the energy barrier for the step-one detwinning, it will fail by planar slip with limited plasticity. Although in the previous study [23] we have come up with a simple energy criterion for the step-one detwinning, it is a very complex process that involves nucleation of multiple dislocations and their reactions with the TB. Many defects such as stacking faults and surface steps created during the step-one detwinning can act as potential sources for shear localization, which will compete with the step-two detwinning under further loading, as shown in Fig. 3. In addition, as shown in Fig. 4, the surface roughness can promote shear localization. In other words, the quality of the step-one detwinning determines whether further tensile detwinning can propagate along the whole NW. However, if we can decouple the step-one and step-two detwinning by directly creating a single-crystalline embryo without any other defects, the bitwinned NW would be expected to be completely detwinned via the step-two detwinning under further loading. We will test this hypothesis in the following.

Figure 5(a)(i) shows a sketch of a pristine bitwinned NW. Similar to the step-one detwinning but by directly manipulating the crystalline structure in MD simulations, we can create a single-crystalline embryo in the middle of the bitwinned NW with the unique TB-GB-TB structure, as shown in Fig. 5(a)(ii). The step-two detwinning can be activated immediately upon further loading. The detailed process of mimicking the step-one detwinning is shown in Fig. 5(b). By cutting the bitwinned NW and welding it with a single-crystalline embryo according to the unique TB-GB-TB structure observed after the step-one detwinning [23], a bitwinned NW with a single-crystalline embryo is constructed without any other defects. The periodic boundary condition is kept in the axial direction by slight tilting the NW to match the two ends and followed an energy minimization process. Figure 6 shows the deformations of three representative NWs with the preconstructed single-crystalline embryo and TB-GB-TB structure. Figure 6(a) mimics the partially detwinned NW previously shown in Fig. 2(a)(ii), by constructing a perfect single-crystalline embryo between the two bitwinned parts. The NW, when subject to step-two detwinning upon further loading, undergoes detwinning along its entire length, in contrast to the shear localization in Fig. 2(a)(ii). In Figs. 6(b)–6(d), we choose three NWs with large volume ratios that were shown unable to detwin due to high activation energy required for step-one detwinning [23]. However, when the single-crystalline embryos are directly constructed, the step-two detwinning becomes the dominant deformation mechanism in all of them. As a result, all NWs are detwinned and fail with large plasticity. Of note is that more and more stacking faults are left in the NW with larger volume ratio, but the original twinned NW can be completely detwinned in all three cases, with plasticity comparable to the single-crystalline case. In addition, if we introduce surface notches that are similar to Fig. 4(a) in the NWs shown in Fig. 6, all of them can still be fully detwinned under tensile loading, which further confirm that if the step-one detwinning is perfectly executed

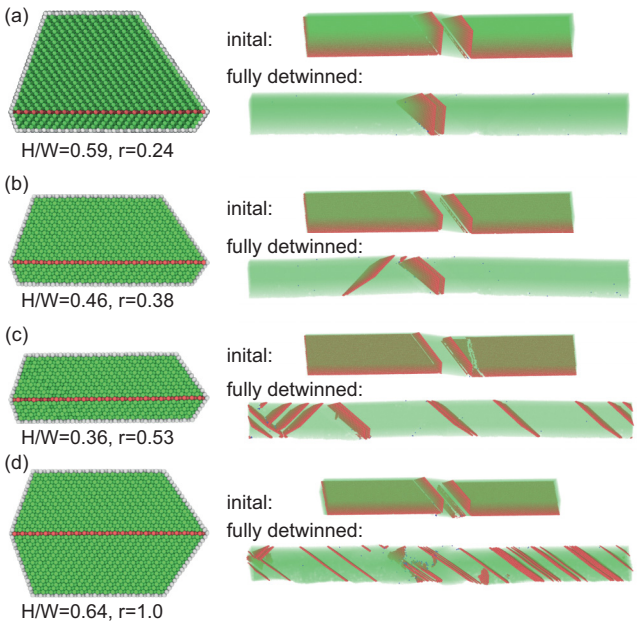

FIG. 6. Step-two detwinning in samples with a directly built-in single-crystalline embryo after step-one detwinning. (a) Through the built-in single-crystalline embryo, the NW undergoes complete tensile detwinning as in Fig. 2(a)(ii) with large plasticity. [(b)–(d)] Bitwinned NWs that cannot overcome the energy barrier for step-one detwinning. When a single-crystalline embryo was directly constructed from crystalline geometry according to Fig. 5, instead of step-one detwinning, the resulting NWs can be fully detwinned via step-two detwinning under tension. Besides EAM potential [46], two other different EAM potentials [47,48] were also adopted here and can get consistent results.

(with no additional dislocations created), tensile detwinning becomes the dominant deformation mechanism regardless of the presence of surface defects.

By directly constructing the single-crystalline embryo without any other defects, all the NWs simulated can be fully detwinned upon tensile loading without considering the activation energy for step-one detwinning. These results further confirm our previous hypothesis about the competition between shear localization and step-two detwinning. Since the single-crystalline embryo is directly constructed instead of through dislocation reactions, there are no other defects in the system to compete with step-two detwinning, in which case the bitwinned NWs are completely detwinned. By decoupling the step-one and step-two detwinning, we thus prove that the nucleation of single-crystalline embryo (step-one detwinning) is the key step to determining the whole deformation mechanism.

D. Tensile detwinning in metallic NWs with multiple TBs running parallel to the length direction

It becomes apparent that tensile detwinning plays an important role for the large plastic deformation in the bitwinned metallic NW with a single TB running parallel to the length direction. Another question is whether, and under what conditions, this delocalized tensile detwinning mechanism can be generalized to other NWs with multiple TBs running parallel to the length direction? Our previous study has shown that the volume ratio between the two twin variants ($r = V_{\text{small}}/V_{\text{large}}$) in bitwinned NWs plays a key role in tensile detwinning [23]. The bitwinned NW with one dominant twin variant (small volume ratio) has lower energy barrier for detwinning. Built upon this idea and inspired by the cross-sectional TEM images of NWs with multiple TBs as shown in Figs. 7(a) and 7(b), we constructed tritwinned (parallel TBs) and asymmetric pentatwinned NWs (intersected TBs) with one dominant twin variant and tested their deformation mechanism in MD simulations. Figures 7(c) and 7(d) show the typical snapshots of a tritwinned NW and an asymmetric pentatwinned NW undergoing tensile detwinning during plastic deformation. The cross sections of these two NWs are shown in Fig. 7(e) along with the corresponding stress-strain curves. It is seen that the original TBs in the NWs are detwinned during the plastic deformation. Similar to the detwinning process in

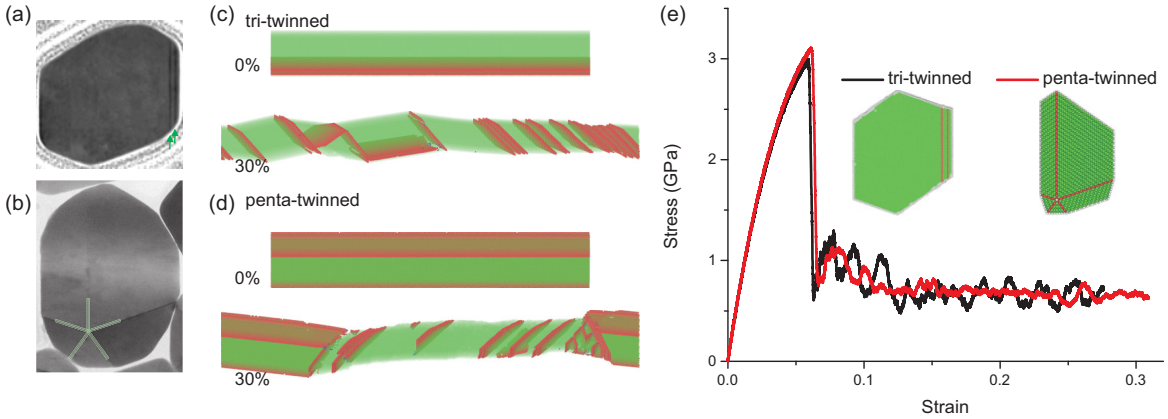

FIG. 7. Tensile detwinning in tritwinned and pentatwinned NWs. (a) TEM cross-section of a tritwinned NW. (b) TEM cross-section of an asymmetric pentatwinned NW. (c) Initial and final configurations of a tritwinned NWs in MD simulation. After 30% strain, most of the original TBs were detwinned. (d) Initial and final configurations of an asymmetric pentatwinned NWs in MD simulation. At 30% strain, most the original TBs were detwinned. (e) Stress strain curves in simulations of (c) and (d). The insets show cross-sections of the tritwinned and asymmetric pentatwinned NWs.

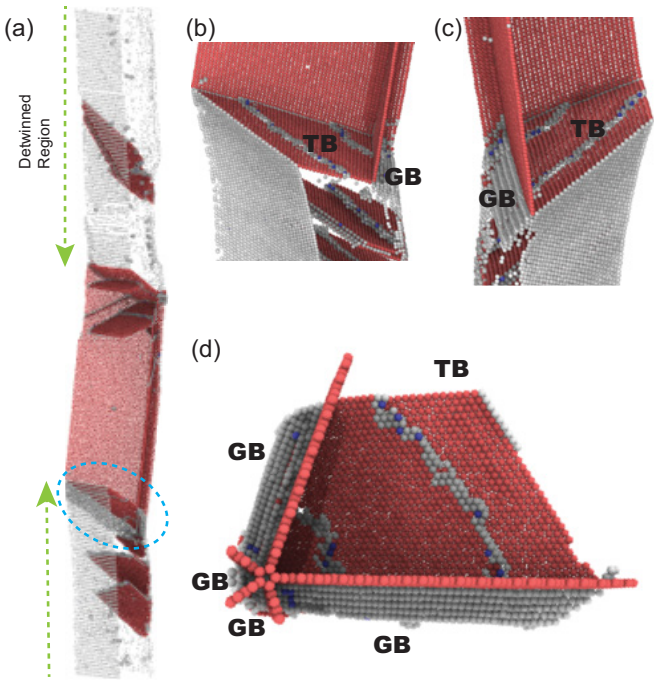

FIG. 8. Detailed structure of tensile detwinning in pentatwinned NWs. (a) Tensile detwinning of a pentatwinned NW. The green dashed line indicates the detwinned region. The blue circle marks the TB-GB structure. [(b) and (c)] Zoom-in view of the connection part between the detwinned single-crystalline and pentatwinned regions. (d) Detailed structure of the newly formed TB-GB structure during the step-one detwinning process.

bitwinned NWs [23], in both NWs partials are first nucleated from the free surface and then propagated into the dominant twin variant. As the partials encounter the TBs, multiple dislocation interactions with the TBs promote the generation of a single-crystalline embryo (step-one detwinning), which further drives the step-two detwinning, leading to large plasticity (see Ref. [54]). The nucleation of a single-crystalline embryo is still the key to subsequent tensile detwinning in the NWs with multiple TBs, which is determined by the cross-sectional aspect ratio and the volume ratio of the dominant twin variant.

Pentatwinned NWs have high yield strength and usually fail by localized necking through nucleation-controlled distributed plasticity [25,52,53]. Here, our MD simulations reveal that tensile detwinning could also occur in asymmetric pentatwinned NWs if one twin variant is dominating, as shown in Fig. 8(a). To systematically investigate the condition of tensile detwinning mechanisms in pentatwinned NWs, a parametric study was conducted in MD simulations. Similar to the bitwinned NWs, after step-one detwinning in pentatwinned NWs, a single-crystalline embryo is formed and the junction between the embryo and the original pentatwinned NWs contains an inclined TB in the dominant twin variant and four high-angle GBs in the other twin variants [Figs. 8(b)–8(d)]. The energy change associated with the step-one detwinning in pentatwinned NWs can be calculated as the energy needed to create the newly formed TB and GBs:

$$\Delta E = 2A_1\gamma_{\text{twin}} + 2A_2\gamma_{\text{GB}}, \tag{1}$$

where A_1 and A_2 are the areas of the TB and the four high-angle GBs as shown in Fig. 8(d), respectively; γ_{twin} and γ_{GB} are the interfacial energies of TB and GB, respectively, with the values of 5.9 and 539 mJ/m^2 obtained from MD simulations.

The inset in Fig. 9(a) shows the cross-section of the simulated pentatwinned NWs, where W, H, and h_1 are the independent geometrical parameters considering the fixed angles of the facets. Note the volume ratio r in pentatwinned NWs, defined as $V_{\text{T1}}/V_{\text{T2}}$, between the two twin variants as shown in Fig. 9(a). For a given value of H, the energy change of the detwinning process ΔE in Eq. (1) can be expressed in terms of two dimensionless parameters: H/W and the volume ratio $r \in (0, 1]$ as

$$\Delta E(A_1, A_2) = \Delta E(W, H, h_1) = \Delta E(H, H/W, r). \tag{2}$$

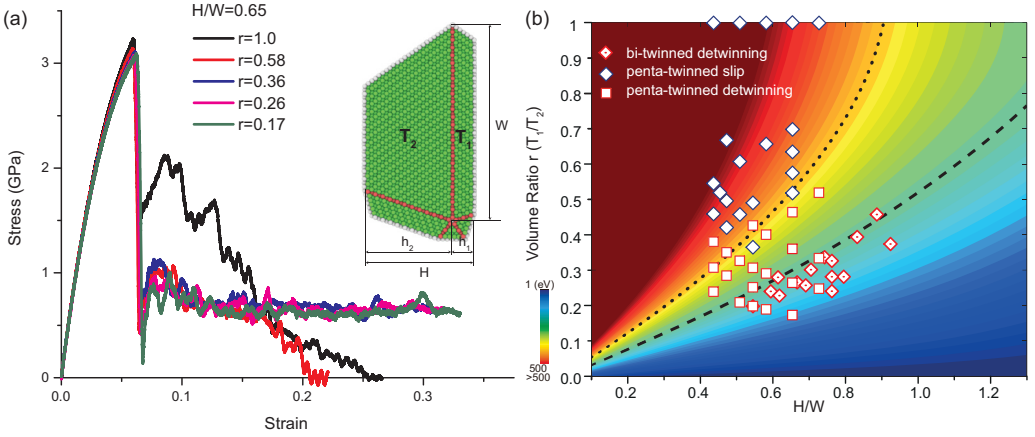

FIG. 9. Slip vs tensile detwinning in pentatwinned NWs. (a), Stress strain curves of pentatwinned NWs with changing twin volume ratio and fixed W and H. When r decreased from 1 to 0.36, the dominant deformation mode transitions from slip to tensile-detwinning. The inset in (a) shows the cross section of a typical pentatwinned NW in MD simulations and its corresponding geometrical parameters. (b) Contour plots of the energy change in the detwinning process for a fixed H as a function of H/W and twin volume ratio r. For comparison, deformation data of bitwinned NWs from previous study [23] are also included on the contour.

Figure 9(a) shows the stress-strain curves of five different pentatwinned NWs with a fixed $H/W = 0.65$ and r ranging from 0.17 to 1.0. For a large volume ratio, e.g., r being 1.0 or 0.58, slip dominates, leading to necking with limited plasticity. However, as r decreases, tensile detwinning mechanism starts to dominate and plateaus in the stress-strain curves can be clearly observed. The NWs with small r fail via tensile detwinning with large plasticity, similar to the case shown in Fig. 7(d).

The contour of ΔE is plotted in Fig. 9(b) for a fixed $H = 8.5$ nm, where the x axis is H/W and the y axis is r. The color from blue to red indicates an increase in ΔE. The value of ΔE varies for different H, but the contour lines are the same regardless of H. The plot shows that pentatwinned NWs with smaller volume ratio and larger H/W have lower energy change, thus favoring tensile detwinning; while those with larger volume ratio and smaller H/W have higher energy change, favoring localized slip. Our simulation results over 40 different pentatwinned NWs, as plotted, show good agreement with the prediction based on ΔE. Besides, results of the bitwinned NWs [with only T_1 and T_2 twin variants as shown in Fig. 9(a)] are also plotted on Fig. 9(b). We can observe that the critical energy difference for the deformation mode transition for pentatwinned NWs [dotted line in Fig. 9(b)] is higher than that for bitwinned NWs [dashed line in Fig. 9(b)], which means that for the same r and H/W, pentatwinned NWs are easier to detwin than bitwinned NWs. A pentatwinned NW can be viewed as equivalent to a bitwinned NW (T_1 and T_2 twin variants) with three extra twin variants. In contrast to the free surfaces in the bitwinned NW, the extra twin variants can facilitate dislocation reactions in the step-one detwinning rather than the dislocation slip. This explains why pentatwinned NWs are more prone to detwinning than bitwinned NW with the same r and H/W parameters.

IV. SUMMARY AND CONCLUSIONS

This study shows that the competition between shear localization and tensile detwinning is the key factor that affects the propagation of tensile detwinning in bitwinned NWs with small volume ratio. By dividing the tensile detwinning process into two steps and studying the progression of each step separately, we found that the quality of the single-crystalline embryo formed during the step-one detwinning process determines the subsequent detwinning propagation and the final extent of plasticity of the NWs. Furthermore, we demonstrated that the two-step tensile detwinning mechanism also works in other metallic NWs with multiple TBs running parallel to the length direction (loading direction), including NWs with three parallel TBs (tritwinned NWs) and asymmetric pentatwinned NWs, each exhibiting remarkable plasticity prior to failure. This work highlights tensile detwinning as an important route for providing large plasticity in metallic NWs with parallel TBs running parallel to the length direction and sheds light on a novel detwinning mechanism in metals.

ACKNOWLEDGMENTS

S.Y. and H.G. acknowledge financial support from NSF through grant DMR-1709318 and computational support by the Extreme Science and Engineering Discovery Environment (XSEDE) through Grant No. MS090046. G.C. and Y.Z. acknowledge financial support from the National Science Foundation (NSF) under Awards No. CMMI-1030637 and No. 1301193. The authors acknowledge the use of the Analytical Instrumentation Facility (AIF) at North Carolina State University, which is supported by the State of North Carolina and the National Science Foundation (Award No. ECCS-1542015). The AIF is a member of the North Carolina Research Triangle Nanotechnology Network (RTNN), a site in the National Nanotechnology Coordinated Infrastructure (NNCI).

[1] E. C. Garnett, W. Cai, J. J. Cha, F. Mahmood, S. T. Connor, M. Greyson Christoforo, Y. Cui, M. D. McGehee, and M. L. Brongersma, Nat. Mater. **11**, 241 (2012).
[2] A. Tao, F. Kim, C. Hess, J. Goldberger, R. He, Y. Sun, Y. Xia, and P. Yang, Nano Lett. **3**, 1229 (2003).
[3] F. Xu and Y. Zhu, Adv. Mater. **24**, 5117 (2012).
[4] W. Wang, Q. Yang, F. Fan, H. Xu, and Z. L. Wang, Nano Lett. **11**, 1603 (2011).
[5] M. Li, R. B. Bhiladvala, T. J. Morrow, J. A. Sioss, K.-K. Lew, J. M. Redwing, C. D. Keating, and T. S. Mayer, Nat. Nanotechnol. **3**, 88 (2008).
[6] J. R. Greer and J. T. M. De Hosson, Prog. Mater Sci. **56**, 654 (2011).
[7] T. Zhu and J. Li, Prog. Mater Sci. **55**, 710 (2010).
[8] C. R. Weinberger and W. Cai, J. Mater. Chem. **22**, 3277 (2012).
[9] Q. Yu, M. Legros, and A. M. Minor, MRS Bull. **40**, 62 (2015).
[10] J. Diao, K. Gall, and M. L. Dunn, Nat. Mater. **2**, 656 (2003).
[11] T. Zhu, J. Li, A. Samanta, A. Leach, and K. Gall, Phys. Rev. Lett. **100**, 025502 (2008).
[12] H. Zheng, A. Cao, C. R. Weinberger, J. Y. Huang, K. Du, J. Wang, Y. Ma, Y. Xia, and S. X. Mao, Nat. Commun. **1**, 144 (2010).
[13] Y. Yue, P. Liu, Q. Deng, E. Ma, Z. Zhang, and X. Han, Nano Lett. **12**, 4045 (2012).
[14] L. Y. Chen, M.-r. He, J. Shin, G. Richter, and D. S. Gianola, Nat. Mater. **14**, 707 (2015).
[15] B. Roos, B. Kapelle, G. Richter, and C. Volkert, Appl. Phys. Lett. **105**, 201908 (2014).
[16] S. Yin, G. Cheng, T.-H. Chang, G. Richter, Y. Zhu, and H. Gao, Nat. Commun. **10**, 2004 (2019).
[17] S. Yin, G. Cheng, G. Richter, H. Gao, and Y. Zhu, ACS Nano **13**, 9082 (2019).
[18] T. H. Chang, G. M. Cheng, C. J. Li, and Y. Zhu, Extreme Mech. Lett. **8**, 177 (2016).
[19] A. M. Minor and G. Dehm, MRS Bull. **44**, 438 (2019).
[20] Y. Zhu, Appl. Mech. Rev. **69**, 010802 (2017).
[21] H. S. Park, K. Gall, and J. A. Zimmerman, J. Mech. Phys. Solids **54**, 1862 (2006).
[22] D. Jang, X. Li, H. Gao, and J. R. Greer, Nat. Nanotechnol. **7**, 594 (2012).
[23] G. Cheng, S. Yin, T.-H. Chang, G. Richter, H. Gao, and Y. Zhu, Phys. Rev. Lett. **119**, 256101 (2017).
[24] S. Narayanan, G. Cheng, Z. Zeng, Y. Zhu, and T. Zhu, Nano Lett. **15**, 4037 (2015).

[25] Q. Qin, S. Yin, G. Cheng, X. Li, T.-H. Chang, G. Richter, Y. Zhu, and H. Gao, Nat. Commun. **6**, 5983 (2015).
[26] R. A. Bernal, A. Aghaei, S. Lee, S. Ryu, K. Sohn, J. Huang, W. Cai, and H. Espinosa, Nano Lett. **15**, 139 (2015).
[27] X. Li, Y. Wei, L. Lu, K. Lu, and H. Gao, Nature (London) **464**, 877 (2010).
[28] K. Lu, L. Lu, and S. Suresh, Science **324**, 349 (2009).
[29] X. Li, S. Yin, S. H. Oh, and H. Gao, Scr. Mater. **133**, 105 (2017).
[30] Q. Huang, D. Yu, B. Xu, W. Hu, Y. Ma, Y. Wang, Z. Zhao, B. Wen, J. He, Z. Liu, and Y. Tian, Nature (London) **510**, 250 (2014).
[31] X. Liu, X. Chen, H.A. Ma, X. Jia, J. Wu, T. Yu, Y. Wang, J. Guo, S. Petitgirard, C.R. Bina, and S.D. Jacobsen, Sci. Rep. **6**, 30518 (2016).
[32] Y. A. Shin, S. Yin, X. Li, S. Lee, S. Moon, J. Jeong, M. Kwon, S.J. Yoo, Y.M. Kim, T. Zhang, H. Gao, and S.H. Oh, Nat. Commun. **7**, 10772 (2016).
[33] J. Wang, F. Sansoz, J. Huang, Y. Liu, S. Sun, Z. Zhang, and S. X. Mao, Nat. Commun. **4**, 1742 (2013).
[34] F. Niekiel, E. Spiecker, and E. Bitzek, J. Mech. Phys. Solids **84**, 358 (2015).
[35] J. Wang and H. Huang, Appl. Phys. Lett. **88**, 203112 (2006).
[36] J. Wang, N. Li, O. Anderoglu, X. Zhang, A. Misra, J. Y. Huang, and J. P. Hirth, Acta Mater. **58**, 2262 (2010).
[37] S. Lee, J. Im, Y. Yoo, E. Bitzek, D. Kiener, G. Richter, B. Kim, and S. H. Oh, Nat. Commun. **5**, 3033 (2014).
[38] Y. T. Zhu, X. L. Wu, X. Z. Liao, J. Narayan, L. J. Kecskés, and S. N. Mathaudhu, Acta Mater. **59**, 812 (2011).
[39] H. Zhou, X. Li, Y. Wang, Z. Liu, W. Yang, and H. Gao, Nano Lett. **15**, 6082 (2015).
[40] Y. M. Wang, F. Sansoz, T. LaGrange, R. T. Ott, J. Marian, T. W. Barbee Jr., and A. V. Hamza, Nat. Mater. **12**, 697 (2013).
[41] G. Richter, K. Hillerich, D. S. Gianola, R. Moenig, O. Kraft, and C. A. Volkert, Nano Lett. **9**, 3048 (2009).
[42] T.-H. Chang and Y. Zhu, Appl. Phys. Lett. **103**, 263114 (2013).
[43] Y. Zhu and H. D. Espinosa, Proc. Natl. Acad. Sci. USA **102**, 14503 (2005).
[44] G. M. Cheng, T. H. Chang, Q. Q. Qin, H. C. Huang, and Y. Zhu, Nano Lett. **14**, 754 (2014).
[45] S. Plimpton, J. Comput. Phys. **117**, 1 (1995).
[46] P. Williams, Y. Mishin, and J. Hamilton, Model. Simul. Mater. Sci. Eng. **14**, 817 (2006).
[47] J. Adams, S. Foiles, and W. Wolfer, J. Mater. Res. **4**, 102 (1989).
[48] Z. Pan, V. Borovikov, M. I. Mendelev, and F. Sansoz, Model. Simul. Mater. Sci. Eng. **26**, 075004 (2018).
[49] S. Nose, J. Chem. Phys. **81**, 511 (1984).
[50] A. Stukowski, Model. Simul. Mater. Sci. Eng. **18**, 015012 (2010).
[51] J.-H. Seo, Y. Yoo, N.-Y. Park, S.-W. Yoon, H. Lee, S. Han, S.-W. Lee, T.-Y. Seong, S.-C. Lee, K.-B. Lee, P.-R. Cha, H.S. Park, B. Kim, and J.-P. Ahn, Nano Lett. **11**, 3499 (2011).
[52] T. Filleter, S. Ryu, K. Kang, J. Yin, R.A. Bernal, K. Sohn, S. Li, J. Huang, W. Cai, and H.D. Espinosa, Small **8**, 2986 (2012).
[53] Y. Zhu, Q. Qin, F. Xu, F. Fan, Y. Ding, T. Zhang, B. J. Wiley, and Z. L. Wang, Phys. Rev. B **85**, 045443 (2012).
[54] See Supplemental Material at http://link.aps.org/supplemental/10.1103/PhysRevMaterials.4.023603 for the movie of tensile detwinning of a pentatwinned NW.